Multistrange Baryon Production in Au-Au Collisions at $\sqrt{s_{NN}} = 130\,\mathrm{GeV}$

J. Adams,[2] C. Adler,[13] M. M. Aggarwal,[28] Z. Ahammed,[42] J. Amonett,[19] B. D. Anderson,[19] D. Arkhipkin,[12]
G. S. Averichev,[11] Y. Bai,[26] J. Balewski,[16] O. Barannikova,[31] L. S. Barnby,[2] J. Baudot,[17] S. Bekele,[27] V.V. Belaga,[11]
R. Bellwied,[45] J. Berger,[13] B. I. Bezverkhny,[47] S. Bharadwaj,[32] V. S. Bhatia,[28] H. Bichsel,[44] L. C. Bland,[3] C. O. Blyth,[2]
B. E. Bonner,[33] M. Botje,[26] A. Boucham,[37] A. Brandin,[24] A. Bravar,[3] R.V. Cadman,[1] X. Z. Cai,[36] H. Caines,[47]
M. Calderón de la Barca Sánchez,[3] J. Carroll,[20] J. Castillo,[20] D. Cebra,[6] P. Chaloupka,[10] S. Chattopdhyay,[42] H. F. Chen,[35]
Y. Chen,[7] J. Cheng,[40] M. Cherney,[9] A. Chikanian,[47] W. Christie,[3] J. P. Coffin,[17] T. M. Cormier,[45] J. G. Cramer,[44]
H. J. Crawford,[5] D. Das,[42] S. Das,[42] M. M. de Moura,[34] A. A. Derevschikov,[30] L. Didenko,[3] T. Dietel,[13] W. J. Dong,[7]
X. Dong,[35] J. E. Draper,[6] F. Du,[47] A. K. Dubey,[14] V. B. Dunin,[11] J. C. Dunlop,[3] M. R. Dutta Mazumdar,[42] V. Eckardt,[22]
L. G. Efimov,[11] V. Emelianov,[24] J. Engelage,[5] G. Eppley,[33] B. Erazmus,[37] M. Estienne,[37] P. Fachini,[3] J. Faivre,[17]
R. Fatemi,[16] J. Fedorisin,[11] K. Filimonov,[20] P. Filip,[10] E. Finch,[47] V. Fine,[3] Y. Fisyak,[3] D. Flierl,[13] K. J. Foley,[3]
K. Fomenko,[11] J. Fu,[40] C. A. Gagliardi,[38] J. Gans,[47] M. S. Ganti,[42] L. Gaudichet,[37] F. Geurts,[33] V. Ghazikhanian,[7]
P. Ghosh,[42] J. E. Gonzalez,[7] O. Grachov,[45] O. Grebenyuk,[26] S. Gronstal,[9] D. Grosnick,[41] S. M. Guertin,[7] A. Gupta,[18]
T. D. Gutierrez,[6] T. J. Hallman,[3] A. Hamed,[45] D. Hardtke,[20] J.W. Harris,[47] M. Heinz,[47] T.W. Henry,[38] S. Hepplemann,[29]
B. Hippolyte,[47] A. Hirsch,[31] E. Hjort,[20] G.W. Hoffmann,[39] H. Z. Huang,[7] S. L. Huang,[35] E. Hughes,[4] T. J. Humanic,[27]
G. Igo,[7] A. Ishihara,[39] P. Jacobs,[20] W.W. Jacobs,[16] M. Janik,[43] H. Jiang,[7] P. G. Jones,[2] E. G. Judd,[5] S. Kabana,[47]
K. Kang,[40] M. Kaplan,[8] D. Keane,[19] V. Yu. Khodyrev,[30] J. Kiryluk,[21] A. Kisiel,[43] E. M. Kislov,[11] J. Klay,[20] S. R. Klein,[20]
A. Klyachko,[16] D. D. Koetke,[41] T. Kollegger,[13] M. Kopytine,[19] L. Kotchenda,[24] M. Kramer,[25] P. Kravtsov,[24]
V. I. Kravtsov,[30] K. Krueger,[1] C. Kuhn,[17] A. I. Kulikov,[11] A. Kumar,[28] C. L. Kunz,[8] R. Kh. Kutuev,[12] A. A. Kuznetsov,[11]
M. A. C. Lamont,[2] J. M. Landgraf,[3] S. Lange,[13] C. L. Lansdell,[39] F. Laue,[3] J. Lauret,[3] A. Lebedev,[3] R. Lednicky,[11]
S. Lehocka,[11] M. J. LeVine,[3] C. Li,[35] Q. Li,[45] Y. LI,[40] S. J. Lindenbaum,[25] M. A. Lisa,[27] F. Liu,[46] L. Liu,[46] Q. J. Liu,[44]
Z. Liu,[46] T. Ljubicic,[3] W. J. Llope,[33] H. Long,[7] R. S. Longacre,[3] M. Lopez-Noriega,[27] W. A. Love,[3] T. Ludlam,[3] D. Lynn,[3]
G. L. Ma,[36] J. G. Ma,[7] Y. G. Ma,[36] D. Magestro,[27] S. Mahajan,[18] D. P. Mahapatra,[14] R. Majka,[47] L. K. Mangotra,[18]
R. Manweiler,[41] S. Margetis,[19] C. Markert,[47] L. Martin,[37] J. N. Marx,[20] H. S. Matis,[20] Yu. A. Matulenko,[30]
C. J. McClain,[1] T. S. McShane,[9] F. Meissner,[20] Yu. Melnick,[30] A. Meschanin,[30] M. L. Miller,[21] Z. Milosevich,[8]
N. G. Minaev,[30] C. Mironov,[19] A. Mischke,[26] D. Mishra,[14] J. Mitchell,[33] B. Mohanty,[42] L. Molnar,[31] C. F. Moore,[39]
M. J. Mora-Corral,[22] D. A. Morozov,[30] V. Morozov,[20] M. G. Munhoz,[34] B. K. Nandi,[42] T. K. Nayak,[42] J. M. Nelson,[2]
P. K. Netrakanti,[42] V. A. Nikitin,[12] L.V. Nogach,[30] B. Norman,[19] S. B. Nurushev,[30] G. Odyniec,[20] A. Ogawa,[3]
V. Okorokov,[24] M. Oldenburg,[20] D. Olson,[20] S. K. Pal,[42] Y. Panebratsev,[11] S. Y. Panitkin,[3] A. I. Pavlinov,[45] T. Pawlak,[43]
T. Peitzmann,[26] V. Perevoztchikov,[3] C. Perkins,[5] W. Peryt,[43] V. A. Petrov,[12] S. C. Phatak,[14] R. Picha,[6] M. Planinic,[48]
J. Pluta,[43] N. Porile,[31] J. Porter,[3] A. M. Poskanzer,[20] M. Potekhin,[3] E. Potrebenikova,[11] B. V. K. S. Potukuchi,[18]
D. Prindle,[44] C. Pruneau,[45] J. Putschke,[22] G. Rai,[20] G. Rakness,[29] R. Raniwala,[32] S. Raniwala,[32] O. Ravel,[37] R. L. Ray,[39]
S. V. Razin,[11] D. Reichhold,[31] J. G. Reid,[44] G. Renault,[37] F. Retiere,[20] A. Ridiger,[24] H. G. Ritter,[20] J. B. Roberts,[33]
O. V. Rogachevskiy,[11] J. L. Romero,[6] A. Rose,[45] L. Ruan,[35] I. Sakrejda,[20] S. Salur,[47] J. Sandweiss,[47] I. Savin,[12]
P. S. Sazhin,[11] J. Schambach,[39] R. P. Scharenberg,[31] N. Schmitz,[22] L. S. Schroeder,[20] K. Schweda,[20] J. Seger,[9]
P. Seyboth,[22] E. Shahaliev,[11] M. Shao,[35] W. Shao,[4] M. Sharma,[28] W. Q. Shen,[36] K. E. Shestermanov,[30] S. S. Shimanskiy,[11]
F. Simon,[22] R. N. Singaraju,[42] G. Skoro,[11] N. Smirnov,[47] R. Snellings,[26] G. Sood,[28] P. Sorensen,[20] J. Sowinski,[16]
J. Speltz,[17] H. M. Spinka,[1] B. Srivastava,[31] L. St. Claire,[20] A. Stadnik,[11] R. Stock,[13] A. Stolpovsky,[45] M. Strikhanov,[24]
B. Stringfellow,[31] C. Struck,[13] A. A. P. Suaide,[34] E. Sugarbaker,[27] C. Suire,[3] M. Sumbera,[10] B. Surrow,[21]
T. J. M. Symons,[20] A. Szanto de Toledo,[34] P. Szarwas,[43] A. Tai,[7] J. Takahashi,[34] A. H. Tang,[26] D. Thein,[7] J. H. Thomas,[20]
S. Timoshenko,[24] M. Tokarev,[11] T. A. Trainor,[44] S. Trentalange,[7] R. E. Tribble,[38] O. Tsai,[7] T. Ullrich,[3] D. G. Underwood,[1]
A. Urkinbaev,[11] G. Van Buren,[3] A. M. Vander Molen,[23] R. Varma,[15] I. M. Vasilevski,[12] A. N. Vasiliev,[30] R. Vernet,[17]
S. E. Vigdor,[16] V. P. Viyogi,[42] S. Vokal,[11] M. Vznuzdaev,[24] B. Waggoner,[9] F. Wang,[31] G. Wang,[19] G. Wang,[4] X. L. Wang,[35]
Y. Wang,[39] Y. Wang,[40] Z. M. Wang,[35] H. Ward,[39] J. C. Webb,[16] R. Wells,[27] G. D. Westfall,[23] A. Wetzler,[20] C. Whitten, Jr.,[7]
H. Wieman,[20] S.W. Wissink,[16] R. Witt,[47] J. Wood,[7] J. Wu,[35] N. Xu,[20] Z. Xu,[35] Z. Xu,[3] E. Yamamoto,[20] P. Yepes,[33]
V. I. Yurevich,[11] Y.V. Zanevsky,[11] H. Zhang,[3] Z. P. Zhang,[35] P. A Zolnierczuk,[16] R. Zoulkarneev,[12]
Y. Zoulkarneeva,[12] and A. N. Zubarev[11]

(STAR Collaboration)*

[1]*Argonne National Laboratory, Argonne, Illinois 60439, USA*
[2]*University of Birmingham, Birmingham, United Kingdom*
[3]*Brookhaven National Laboratory, Upton, New York 11973, USA*
[4]*California Institute of Technology, Pasedena, California 91125, USA*
[5]*University of California, Berkeley, California 94720, USA*
[6]*University of California, Davis, California 95616, USA*
[7]*University of California, Los Angeles, California 90095, USA*
[8]*Carnegie Mellon University, Pittsburgh, Pennsylvania 15213, USA*
[9]*Creighton University, Omaha, Nebraska 68178, USA*
[10]*Nuclear Physics Institute AS CR, Řež/Prague, Czech Republic*
[11]*Laboratory for High Energy (JINR), Dubna, Russia*
[12]*Particle Physics Laboratory (JINR), Dubna, Russia*
[13]*University of Frankfurt, Frankfurt, Germany*
[14]*Insitute of Physics, Bhubaneswar 751005, India*
[15]*Indian Institute of Technology, Mumbai, India*
[16]*Indiana University, Bloomington, Indiana 47408, USA*
[17]*Institut de Recherches Subatomiques, Strasbourg, France*
[18]*University of Jammu, Jammu 180001, India*
[19]*Kent State University, Kent, Ohio 44242, USA*
[20]*Lawrence Berkeley National Laboratory, Berkeley, California 94720, USA*
[21]*Massachusetts Institute of Technology, Cambridge, Massachusetts 02139-4307, USA*
[22]*Max-Planck-Institut für Physik, Munich, Germany*
[23]*Michigan State University, East Lansing, Michigan 48824, USA*
[24]*Moscow Engineering Physics Institute, Moscow, Russia*
[25]*City College of New York, New York City, New York 10031, USA*
[26]*NIKHEF, Amsterdam, The Netherlands*
[27]*The Ohio State University, Columbus, Ohio 43210, USA*
[28]*Panjab University, Chandigarh 160014, India*
[29]*Pennsylvania State University, University Park, Pennsylvania 16802, USA*
[30]*Institute of High Energy Physics, Protvino, Russia*
[31]*Purdue University, West Lafayette, Indiana 47907, USA*
[32]*University of Rajasthan, Jaipur 302004, India*
[33]*Rice University, Houston, Texas 77251, USA*
[34]*Universidade de Sao Paulo, Sao Paulo, Brazil*
[35]*University of Science & Technology of China, Anhui 230027, China*
[36]*Shanghai Institute of Applied Physics, Shanghai 201800, People's Republic of China*
[37]*SUBATECH, Nantes, France*
[38]*Texas A&M, College Station, Texas 77843, USA*
[39]*University of Texas, Austin, Texas 78712, USA*
[40]*Tsinghua University, Beijing, People's Republic of China*
[41]*Valparaiso University, Valparaiso, Indiana 46383, USA*
[42]*Variable Energy Cyclotron Centre, Kolkata 700064, India*
[43]*Warsaw University of Technology, Warsaw, Poland*
[44]*University of Washington, Seattle, Washington 98195, USA*
[45]*Wayne State University, Detroit, Michigan 48201, USA*
[46]*Institute of Particle Physics, CCNU (HZNU), Wuhan 430079, China*
[47]*Yale University, New Haven, Connecticut 06520, USA*
[48]*University of Zagreb, Zagreb HR-10002, Croatia*

The transverse mass spectra and midrapidity yields for Ξs and Ωs are presented. For the 10% most central collisions, the $\overline{\Xi}^+/h^-$ ratio increases from the Super Proton Synchrotron to the Relativistic Heavy Ion Collider energies while the Ξ^-/h^- stays approximately constant. A hydrodynamically inspired model fit to the Ξ spectra, which assumes a thermalized source, seems to indicate that these multistrange particles experience a significant transverse flow effect, but are emitted when the system is hotter and the flow is smaller than values obtained from a combined fit to π, K, p, and Λs.

In heavy ion collisions, we aim to investigate nuclear matter under extreme conditions of pressure and temperature which is expected to lead to the creation of deconfined partonic matter, the quark gluon plasma [1]. Copious partonic interactions will dominate the early stage of the collision should such a thermalized state occur, which will lead to collective partonic effects. The system, as reflected by the observed hadrons, will show a significant

fraction of transverse flow and characteristics of equilibration coming from the partonic phase.

In high energy collisions, the production of strangeness through partonic interactions, mainly $gg \rightarrow s\bar{s}$, may allow the system to reach strangeness saturation (i.e., complete chemical equilibrium) in both the partonic and the hadronic phase [2,3]. The presence of chemical equilibrium at the chemical freeze-out can be inferred from statistical model fits to the particle ratios [4–8] and, in particular, to those involving multistrange baryons [7,9].

The collective partonic effects in the early stage of the collision will contribute to the total observed transverse flow, as it is a cumulative effect. It has previously been suggested that thermal freeze-out occurs much earlier for Ωs and Ξs than for non- or single-strange particles due to the predicted low scattering cross section of Ω and Ξ [10]. In the limit of vanishing cross sections, this would mean that these particles are emitted almost directly from the phase boundary of the hadronizing fireball and carry transverse flow information of an earlier stage of the collision than that of the lighter mass particles. Thus multistrange baryons might be an important probe to identify a possible contribution to the observed transverse flow from the early partonic stage.

In this Letter we present multistrange baryons, Ξ and Ω, transverse mass spectra as measured by the STAR detector in Au + Au collisions at $\sqrt{s_{NN}} = 130$ GeV. The main tracking detector is a large cylindrical time projection chamber. A central trigger barrel measuring the produced charged particle multiplicity around midrapidity plus two zero degree calorimeters measuring neutral spectator energy were used for triggering [11]. The centrality of the collisions is determined from the measured midrapidity negative particle multiplicity. The data were divided into three centrality classes corresponding to 0%–10%, 10%–25%, and 25%–75% of the total hadronic cross section as described in [12]. Multistrange particles are identified via their decay modes $\Xi \rightarrow \Lambda + \pi$ and $\Omega \rightarrow \Lambda + K$ with the subsequent decay of $\Lambda \rightarrow p + \pi$. The tertiary Λ vertex is identified by selecting positive and negative tracks that are consistent with an origin at the decay of a hyperon some distance from the primary collision point [13]. The secondary vertex of the decay is located in a similar fashion by combining the previously identified Λ with a charged particle. Simple cuts on geometry, kinematics, and particle identification, via specific ionization, are applied at each step to reduce the background due to the high multiplicity [12]. The momenta of the daughter particles at the decay vertex are then combined to calculate the parent particle kinematics. The peaks (HWHM ~ 5 MeV$/c^2$) in the invariant mass plots have a signal to noise ratio of 0.74, 0.78, and 0.86 for the Ξ^-, $\overline{\Xi}^+$, and Ω, respectively, in the 0%–10% centrality bin. The signal is calculated from the invariant mass distribution by counting the entries within ± 15 MeV$/c^2$ about the expected mass and then subtracting the background [14]. The back-

ground is estimated by sampling two regions on either side of the peak. The statistics of the Ω^- and $\overline{\Omega}^+$ signals are not sufficient to allow a separate measurement of the spectra of each particle. Hence Ω refers to $\Omega^- + \overline{\Omega}^+$. The momentum integrated $\overline{\Omega}^+/\Omega^-$ ratio for the top 11% most central data is 0.95 ± 0.15(stat) ± 0.05(syst) [14].

The invariant mass distributions are histogrammed in transverse mass, $m_\perp = \sqrt{p_\perp^2 + m^2}$, and the signal extracted for each bin as described above. The raw yield in each $m_\perp$ bin is then corrected for detector acceptance and reconstruction efficiency by the Monte Carlo technique, where simulated particles were embedded into real events. The data cover $|y| < 0.75$, where efficiency and acceptance studies have shown the corrections to be constant. The total acceptance and efficiency for the $\Xi(\Omega)$ are 0.2% (0.04%) for the lowest $m_\perp$ bin rising to 4.0% (0.5%) for the highest bin.

Figure 1 shows the invariant $m_\perp$ spectra as function of centrality for Ξ^- and $\overline{\Xi}^+$, and Ω for the 10% most central data. Systematic uncertainties, principally due to low $p_\perp$ single track reconstruction and background determination, are a function of $p_\perp$. They drop from ~15% at low $p_\perp$ to a few percent at $p_\perp > 1.5$ GeV$/c$. This uncertainty is added in quadrature, on a bin-by-bin basis, to the statistical one, yielding the vertical bars in Fig. 1. We estimate the remaining systematic uncertainties to be 10% on both the extracted invariant yields and slope parameters, the major source of which lies in the misrepresentation of the embedded Monte Carlo to the data resulting in a systematic uncertainty in the efficiency calculation. These were obtained by exploring the dependence of the invariant yields and slope parameters to changes in the cuts phase space (more details can be found in
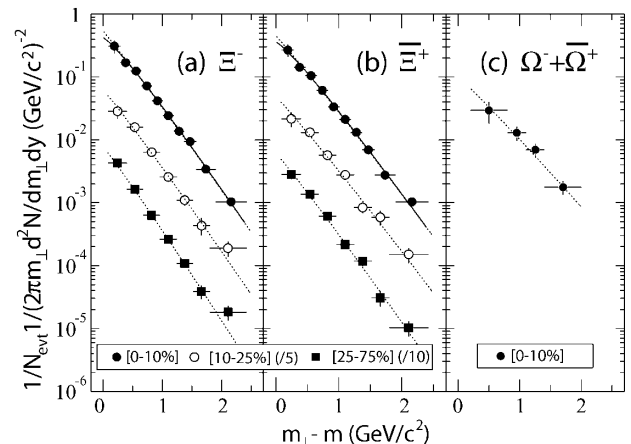

FIG. 1. $m_\perp$ spectra for (a) Ξ^-, (b) $\overline{\Xi}^+$, and (c) Ω as a function of centrality. Scale factors have been applied to the spectra for clarity. Points are drawn at the bin center. The horizontal bars indicate the bin size. The dashed curves are Boltzmann fits to the spectra. The solid curves are hydrodynamically inspired model fits to the most central Ξ^- and $\overline{\Xi}^+$ spectra.

TABLE I. Fit parameters for the $m_\perp$ spectra of the Ξ^-, $\overline{\Xi}^+$, and Ω. The data represent the 0%–10%, 10%–25%, and 25%–75% centrality bins with $h^- = dN_{h^-}/d\eta|_{|\eta|<0.5}$. Only statistical and $p_\perp$ dependent systematic uncertainties are presented. The $p_\perp$ independent systematic uncertainties are 10%.

Centrality (h^-)		Exponential		Boltzmann	
		dN/dy	T_E(MeV)	dN/dy	T_B(MeV)
0%–10% (260.3 ± 7.5)	Ξ^-	2.04 ± 0.14	338 ± 6	2.00 ± 0.14	296 ± 5
	$\overline{\Xi}^+$	1.74 ± 0.12	339 ± 7	1.70 ± 0.12	297 ± 5
	Ω	0.56 ± 0.11	417 ± 52	0.55 ± 0.11	362 ± 39
10%–25% (163.6 ± 5.2)	Ξ^-	1.16 ± 0.12	335 ± 16	1.14 ± 0.12	291 ± 13
	$\overline{\Xi}^+$	0.94 ± 0.10	349 ± 17	0.93 ± 0.10	302 ± 13
25%–75% (42.5 ± 3.0)	Ξ^-	0.29 ± 0.02	312 ± 12	0.28 ± 0.02	273 ± 10
	$\overline{\Xi}^+$	0.22 ± 0.02	320 ± 11	0.22 ± 0.02	280 ± 9

[15,16,17]). The weak decay feeddown of Ω to Ξ is estimated to be less than 2% and thus is neglected.

Table I shows the results of fitting the $m_\perp$ spectra by exponential ($A_E e^{-(m_\perp-m)/T_E}$) and Boltzmann ($A_B m_\perp e^{-(m_\perp-m)/T_B}$) functions. For the 10% most central collisions, the χ^2/d.o.f. are 9.8/8 and 7.4/8 for the exponential and the Boltzmann fits to the Ξ^- spectra and 1.5/2 and 1.3/2 for fits to the Ω spectra. Similar values are obtained for the $\overline{\Xi}^+$ and the other centralities. The inverse slopes of the Ξ^- and $\overline{\Xi}^+$ particles are the same within uncertainties and show no apparent increase over the measured centralities. The yields per unit of rapidity are extracted by summing the fiducial yields and the integral of each function over the unmeasured $m_\perp$ ranges. The measured Ξ spectra correspond to ~80% of the total yield and the Ω to ~66%. The Ξ^- and $\overline{\Xi}^+$ yields as a function of $h^- = dN_{h^-}/d\eta|_{|\eta|<0.5}$ appear linear; such behavior was reported for the Λ hyperon at the Relativistic Heavy Ion Collider (RHIC) [13].

The $\overline{\Xi}^+/h^-$ and $\overline{\Lambda}/h^-$ ratios for the most central data, as shown in Fig. 2(a), increase from Super Proton Synchrotron (SPS) energies [18] to RHIC, whereas the

FIG. 2. (a) Ξ^-, $\overline{\Xi}^+$, Λ, and $\overline{\Lambda}$ to h^- ratios and (b) Ξ^-/Λ and $\overline{\Xi}^+/\overline{\Lambda}$ ratios for the most central data as a function of $\sqrt{s_{NN}}$. The solid bars indicate the statistical uncertainty while the caps indicate the statistical and systematic uncertainties added in quadrature. Some ratios are slightly shifted along the x axis for clarity.

Ξ^-/h^- ratio stays constant and the Λ/h^- decreases. When discussing the baryon ratios, the interplay of increased strangeness production and reduction in the net-baryon number from SPS to RHIC has to be considered. The proximity of the net-baryon number to zero at RHIC is reflected in the fact that the ratio of Ξ^-/h^- is close to $\overline{\Xi}^+/h^-$. The reduction in the net-baryon number has a larger effect on the Λ than on the Ξ^-, as seen in Fig. 2(a), and thus creates the observed rise in the Ξ^-/Λ ratio [Fig. 2(b)]. It is interesting to note that the $\overline{\Xi}^+/\overline{\Lambda}$ ratio is constant from SPS to RHIC, indicating that the scale of the enhancement is the same for singly and doubly strange baryons. The Ξ/Λ ratios are feeddown corrected from weak decay of Ξ to Λ [13].

A fit to the reported 0%–10% centrality particle ratios from STAR [13,14,19–22], including these multistrange particle measurements, using the thermal model described in [8] results in a χ^2/d.o.f. of 8.5/9, a chemical freeze-out temperature (T_{ch}) of 181 ± 8 MeV, light quark and strange quark chemical potentials of 11.7 ± 0.6 and 0.9 ± 1.6 MeV, respectively, and a strangeness saturation factor $\gamma_s = 0.96 \pm 0.06$. First, we note (as previously observed [23]) how remarkably close is the obtained T_{ch} to the phase transition from lattice QCD calculations [24]. Second, the fact that γ_s is equal to unity, within errors, when used as a free parameter in the model indicates that a saturation of strangeness production [8,9] has been achieved in the most central collisions. Table II shows particle ratios for the 0%–10% centrality bin compared to values from three different models: a fit corresponding to the statistical model used above, another corresponding to a statistical model that allows, and obtains, chemical nonequilibrium via an over-saturation of the strangeness phase space [9], and the prediction of the event generator HIJING/$B\overline{B}$ v1.0 which uses a gluon-junction mechanism to enhance the transport of baryons to midrapidity [25]. All ratios are well reproduced by both statistical models, indicating that the strangeness production appears to be at least saturated, and thus suggesting that efficient strangeness production channels are present
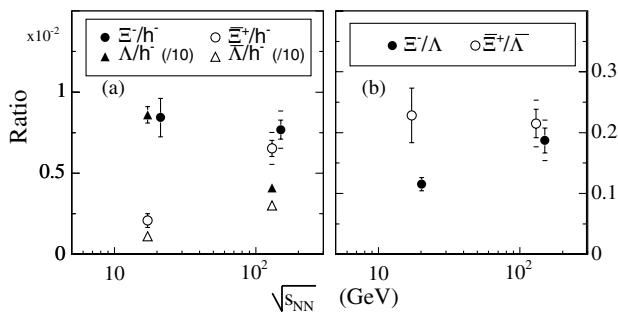
TABLE II. Ratios from the 10% most central data compared to predictions from a statistical model [8], a nonequilibrium model [9], and HIJING/$B\overline{B}$ [25]. The uncertainties shown are first statistical and then systematic.

Ratio ($\times 10^{-3}$)	Data 0%–10%	Stat.	Nonequil.	HIJING/$B\overline{B}$
Ξ^-/h^-	$7.7 \pm 0.6 \pm 1.0$	7.7	7.6	5.1
$\overline{\Xi}^+/h^-$	$6.5 \pm 0.5 \pm 0.8$	6.5	6.1	3.0
Ω/h^-	$2.1 \pm 0.4 \pm 0.4$	2.9	2.8	0.29
Ξ^-/Λ	$187 \pm 20 \pm 26$	148	190	171
$\overline{\Xi}^+/\overline{\Lambda}$	$215 \pm 24 \pm 30$	163	207	142

in the early stages of central collisions. HIJING/$B\overline{B}$, however, fails to predict the multistrange to h^- ratios, in particular, that of the Ω, which it underpredicts by nearly an order of magnitude. It has previously been shown that HIJING successfully predicts the midrapidity total charged particle yields [26], suggesting that the entropy is reasonably well reproduced by this model. The addition of the gluon-junction mechanism, which was necessary to replicate the small net-baryon yields at RHIC [27], does not sufficiently enhance the multistrange baryon yields. A different physics mechanism is thus necessary to model the strangeness production. At SPS energies the introduction of final state interactions helped to account for the observed hyperon enhancement but failed to reproduce the overall strangeness production (K^+/π^+) [28]. The introduction of strong partonic interactions in the initial state was needed to account for both the hyperon and overall strangeness production at the SPS [29].

After reporting the yields to study the chemical content of the system, we address now the thermal freeze-out properties of the multistrange baryons. For this purpose,

we fit the 10% most central $m_\perp$ spectra to a hydrodynamically inspired function [30]. In this model, all considered particles are emitted from a thermal expanding source with a transverse flow velocity $\langle \beta_\perp \rangle$ at the thermal freeze-out temperature T_{fo}. We use a flow velocity profile of $\beta_\perp(r) = \beta_s(r/R)^n$, where R is the maximum emission radius and $n = 0.5$ (as in [20]), and a constant particle density profile. The dashed lines of Fig. 3(a) show the one, two, and three sigma contours for T_{fo} versus $\langle \beta_\perp \rangle$ for the fit to the Ξ^- and $\overline{\Xi}^+$ data combined, with the diamond indicating the best fit solution ($T_{\text{fo}} = 182 \pm 39$ MeV, $\langle \beta_\perp \rangle = (0.42 \pm 0.08)c$, and $\chi^2/\text{d.o.f.} = 13/15$). Also shown, as solid lines, are the one, two, and three sigma contours for a combined fit to the STAR π, K, p, and Λ data [13,20–22]. The marker is the optimal fit location. In varying the velocity profile from $n = 0.5$ to $n = 1.0$, T_{fo} decreases by $\sim 15\%$ and $\langle \beta_\perp \rangle$ remains constant ($\sim 1\%$). For $n > 1.0$, the fit does not reproduce the light particles spectra anymore [20]. No significant effect is seen in [31] for several variations of the particle density profile. In all the cases, the results for the two data sets do not overlap, indicating that the Ξ baryons, within this approach, show a different thermal freeze-out behavior than π, K, p, and Λ. The current Ω statistics do not allow one to distinguish between an early decoupling or a common freeze-out with the lighter species. Figure 3(b) shows the mean $p_\perp$ for these particles calculated from the functions which best reproduce each $m_\perp$ spectrum (Bose-Einstein for π, exponential for K, hydrodynamically inspired function for p, and Boltzmann for Λ, Ξ, and Ω). The error bars are statistical, and systematic uncertainties added in quadrature. The band represents the model prediction based on the three sigma contour for the fit to the STAR π, K, p, and Λ data, while the lower dashed curve shows the prediction for $T_{\text{fo}} = 170$ MeV, $\langle \beta_\perp \rangle = 0$, i.e., a system
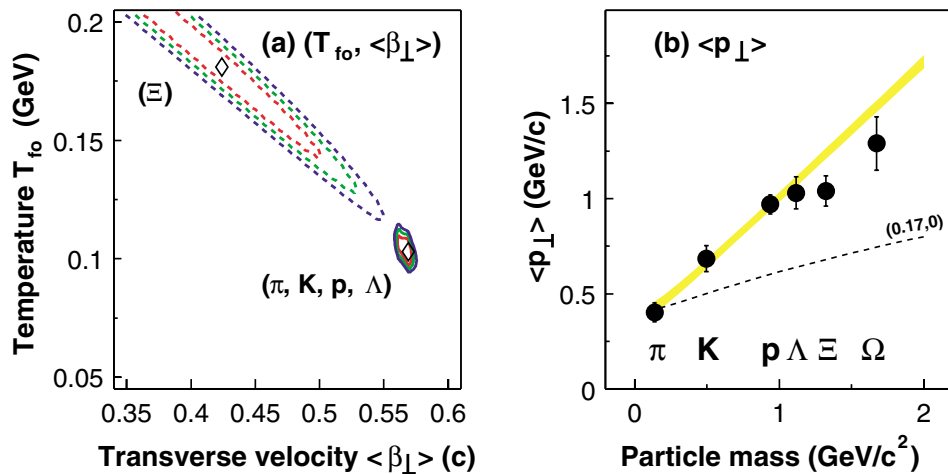

FIG. 3 (color online). (a) T_{fo} versus $\langle \beta_\perp \rangle$ for the hydrodynamically inspired model fits to the $m_\perp$ spectra. The one, two, and three sigma contours are shown. Dashed curves are for a simultaneous fit to the Ξ^- and $\overline{\Xi}^+$. Solid curves are a separate fit to the STAR π, K, p, and Λ data. The diamonds represent the best fit in both cases. (b) $\langle p_\perp \rangle$ for identified particles versus particle mass (see text for details). The band results from the three sigma contour of the hydrodynamically inspired model fit to the π, K, p, and Λ data, and the dashed curve is for $T_{\text{fo}} = 170$ MeV, $\langle \beta_\perp \rangle = 0$.

where thermal and chemical freeze-out coincide and no transverse flow is developed. From Fig. 3(a) it is likely that the Ξ baryons prefer a hotter thermal freeze-out temperature parameter and a smaller transverse flow velocity, when compared to those resulting from fits to the lower mass particles. This is consistent with the calculated $\langle p_\perp \rangle$ of the Ξ being below the solid band in Fig. 3(b). Although from the current statistics we cannot draw any conclusion for the Ω, Fig. 3(b) suggests they behave as the Ξ.

If, as indicated by the hydroinspired fit, the Ξ thermal freeze-out occurs in conjunction with that of chemical freeze-out, $T_{ch} \sim 170$ MeV, this could be an indication that a significant fraction of the collective transverse flow has already developed at/before chemical freeze-out, probably at a partonic stage. A similar picture, although with lower flow, has been suggested for Ω, J/Ψ, and Ψ' at SPS energies [32]. Two alternative models have also been proposed for describing the RHIC spectra. The first [33] assumes that all transverse radial flow is developed at/ before $T_{ch} = T_{fo} = 165$ MeV. The apparent softening of the lighter mass spectra is then due to contamination from resonance decay products. A hydrodynamical approach with a partonic and a hadronic phase [34] is used in the second scenario where the particle mean free paths are assumed small until thermal freeze-out around $T_{fo} = 110$ MeV. These large cross sections result in even the Ω developing a fraction of its radial flow after hadronization. We note that in those three scenarios a significant fraction, if not all, of the observed transverse flow for multistrange baryons is developed prior to chemical freeze-out.

In summary, the yield of multistrange antibaryons per h^- is increased compared to top SPS energies, while the ratio of Ξ^-/h^- stays approximately constant. A chemical analysis of the data indicates that for central collisions the strangeness phase space is now saturated. A fit of the $m_\perp$ spectra to a hydrodynamically inspired model suggests the Ξ baryons thermally freeze-out of the rapidly expanding collision region at a hotter temperature, which is close to that of chemical freeze-out, and with a smaller transverse flow than the lighter particle species. This suggests that they decouple at an earlier stage of the collision and thus probe a different dynamical region, but one at which a sizable fraction of the transverse flow has already developed.

*Electronic address: www.star.bnl.gov
[1] For reviews and recent developments, see Special issue on *Quark Matter 2002* [Nucl. Phys. **A715**, 1c (2003)].
[2] J. Rafelski and B. Müller, Phys. Rev. Lett. **48**, 1066 (1982).
[3] P. Koch, B. Müller, and J. Rafelski, Phys. Rep. **142**, 167 (1986).
[4] P. Braun-Munzinger et al., Phys. Lett. B **344**, 43 (1995).
[5] A. Keranen and F. Becattini, Phys. Rev. C **65**, 044901 (2002).
[6] P. Braun-Munzinger et al., Phys. Lett. B **465**, 15 (1999).
[7] P. Braun-Munzinger et al., Phys. Lett. B **518**, 41 (2001).
[8] N. Xu and M. Kaneta, Nucl. Phys. **A698**, 306 (2002).
[9] J. Rafelski and J. Letessier, Nucl. Phys. **A715**, 98 (2003).
[10] H. van Hecke, H. Sorge, and N. Xu, Phys. Rev. Lett. **81**, 5764 (1998).
[11] STAR Collaboration, M. Anderson et al., Nucl. Instrum. Methods Phys. Res., Sect. A **499**, 659 (2003).
[12] C. Adler et al., Phys. Rev. Lett. **87**, 112303 (2001).
[13] C. Adler et al., Phys. Rev. Lett. **89**, 092301 (2002).
[14] J. Adams et al., Phys. Lett. B **567**, 167 (2003).
[15] C. Lansdell, Ph.D. thesis, University of Texas, 2002.
[16] J. Castillo, Ph.D. thesis, Université de Paris 7, 2002.
[17] B. Hippolyte, Ph.D. thesis, Université de Strasbourg, 2002.
[18] E. Andersen et al., J. Phys. G **25**, 171 (1999).
[19] C. Adler et al., Phys. Rev. C **65**, 041901(R) (2002).
[20] J. Adams et al., nucl-ex/0306029.
[21] C. Adler et al., nucl-ex/0206008.
[22] J. Adams et al., nucl-ex/0311017.
[23] P. Braun-Munzinger and J. Stachel, J. Phys. G **28**, 1971 (2002).
[24] F. Karsch, Nucl. Phys. **A698**, 199 (2002).
[25] X. N. Wang and M. Gyulassy, Phys. Rev. D **44**, 3501 (1991); S. E. Vance et al., Phys. Lett. B **443**, 45 (1998).
[26] B. B. Back et al., Phys. Rev. Lett. **87**, 102303 (2001).
[27] K. Adcox et al., Phys. Rev. Lett. **89**, 092302 (2002).
[28] S. V. Afanasiev, Phys. Rev. C **66**, 054902 (2002).
[29] S. Vance, J. Phys. G **27**, 603 (2001).
[30] E. Schnedermann, J. Sollfrank, and U. Heinz, Phys. Rev. C **48**, 2462 (1993).
[31] K. Adcox et al., Phys. Rev. C **69**, 024904 (2004).
[32] K. A. Bugaev, M. Gazdzicki, and M. I. Gorenstein, Phys. Rev. Lett. **88**, 132301 (2002).
[33] W. Broniowski and W. Florkowski, Phys. Rev. Lett. **87**, 272302 (2001).
[34] P. F. Kolb and U. Heinz, nucl-th/0305084.